A candidate fusion engineering material, WC-FeCr

Humphry-Baker, Samuel A.; Harrison, Robert W.; Greaves, Graeme; Knowles, Alexander J.; Smith, George D.W.; Donnelly, Stephen E.; Lee, William E.

[Link to publication on Research at Birmingham portal](#)

Regular article

A candidate fusion engineering material, WC-FeCr

Samuel A. Humphry-Baker [a,*], Robert W. Harrison [b], Graeme Greaves [b], Alexander J. Knowles [a], George D.W. Smith [c], Stephen E. Donnelly [b], William E. Lee [a,d]

[a] Centre for Nuclear Engineering, Department of Materials, Imperial College London, SW7 2BP, UK
[b] School of Computing and Engineering, University of Huddersfield, HD1 3DH, UK
[c] Tokamak Energy Ltd., 120A Olympic Avenue, Milton Park, Oxfordshire OX1 4SA, UK
[d] Nuclear Futures Institute, Bangor University, Bangor, Gwynedd LL57 1UT, UK

ARTICLE INFO

ABSTRACT

A new candidate fusion engineering material, WC-FeCr, has been irradiated with He ions at 25 and 500 °C. Ions were injected at 6 keV to a dose of ~15 dpa and 50 at. % He, simulating direct helium injection from the plasma. The microstructural evolution was continuously characterised in situ using transmission electron microscopy. In the FeCr phase, a coarse array of 3–6 nm bubbles formed. In the WC, bubbles were less prominent and smaller (~2 nm). Spherical-cap bubbles formed at hetero-phase interfaces of tertiary precipitates, indicating that enhanced processing routes to minimise precipitation could further improve irradiation tolerance.
© 2018 Acta Materialia Inc. Published by Elsevier Ltd. This is an open access article under the CC BY license (http://creativecommons.org/licenses/by/4.0/).

The leading candidates for plasma facing materials (PFMs) in tokamak fusion power plants are tungsten and its alloys. The inherent brittleness of metallic tungsten [1] precludes its use in many structural applications, which has sparked research into tungsten-based composites with enhanced ductility. Recent approaches include fibre-reinforced tungsten [2], tungsten heavy alloys [3] and tungsten laminates [4]. One candidate class of materials that are widely employed in the extreme wear environments, but are as yet little explored as PFMs, is WC-composites. These materials possess excellent neutronics [5] and mechanical [6] properties, while they can be fabricated and shaped inexpensively. A particularly promising binder is the FeCr system, as it is low-activation and resistant to dry oxidation and irradiation.

Like all candidate PFMs a major concern with WC-FeCr composites is how their properties degrade under irradiation, in particular under helium bombardment. Helium will accumulate in PFMs via two mechanisms: firstly via (n, α) transmutation reactions and secondly from direct injection of helium ash from the fusion plasma, particularly in the near-surface region. Both processes can lead to formation of helium bubbles and associated defect structures (interstitial-vacancy pairs, dislocation loops, etc.). While these processes are well understood in many structural nuclear materials [7], they are as yet unstudied for WC-composites.

The general understanding of ion-irradiation in WC-composites is restricted mostly to surface hardening produced by N^{x+} ions on WC-Co (i.e. non fusion-compatible) materials [8]. Whilst the extent to which these studies pertain to helium irradiation or WC-FeCr is limited, we nevertheless discuss the general observations here. Most studies, typically employing 50–100 keV ions, report a two-stage microstructure-property evolution with dose: an initial increase in defect content, with a corresponding hardening, peaking at a dose of $\sim10^{17}$ ions/cm^2. Hardening is attributed to nitride particles forming within the binder [9] and high densities of dislocations and planar defects within WC particles [10]. Defect density is strongly dependent on particle orientation relative to the ion-beam [11]. This hardening is followed by softening due to amorphization of WC. Since the nitrogen is soluble (unlike helium), bubbles are never observed.

Irradiation of WC-composites with He^{x+}, on the other hand, is relatively poorly understood. Available information is limited to mechanical property evolution and in WC-Co only. For example, when irradiated with 32 MeV ions to $\sim1 \times 10^{17}$ ions/cm^2, the surface hardness rises monotonically up to a 30% increase [12, 13]. These surface measurements were not on the helium accumulated region of the specimen (~100 μm below) and no microstructural observations were made. While some speculation about the performance of WC-FeCr can be made from previous studies of its constituents (e.g. monolithic Fe-Cr alloys [14, 15]) such predictions are limited, since there is currently little understanding reported on the response of metal-ceramic interfaces, which – as we will show here – can dominate microstructural evolution.

In what follows, we report He ion irradiation with in-situ transmission electron microscopy (TEM) on a WC-FeCr composite. Irradiations were performed at room temperature and 500 °C (a local maximum

Table 1
Maxima in displacement damage and injected helium, as predicted from SRIM (ions), compared to FISPACT-II simulations (neutrons).

Phase	Neutron dpa	Ion dpa	Neutron He (at. %)	Ion He (at. %)
WC	10	15	0.020	49
FeCr	16	16	0.019	48

for swelling in ion-irradiated FeCr alloys [15]). Bubble size is reported as a function of irradiation dose and temperature. Large bubbles are observed at the interface of impurity phases, which could significantly embrittle the material. Our observations enable processing recommendations for removing these phases and thus enhancing the material's irradiation tolerance.

Tungsten carbide composite plate was obtained from Sandvik Hyperion Ltd. It was manufactured via a conventional liquid phase sintering process, details of which can be found elsewhere [16]. The material contained a nominal weight fraction of 0.9 WC particles and 0.1 Fe-Cr binder, which itself had respective weight fractions of 0.92 Fe and 0.08 Cr. A Cr fraction of 0.08 was selected as an intermediary value between 0.05 and 0.09 – which are known local minima in FeCr alloys for void swelling [15] and ductile-brittle transition temperature [17], respectively.

TEM samples were prepared using an FEI Quanta dual beam Focused Ion Beam system employing Ga ions. Ion-irradiations were performed at the Microscope and Ion Accelerator for Materials Investigations (MIAMI) facility, details of which are given elsewhere [18]. Bright-field (BF) images were collected using a JEOL JEM-2000FX TEM, operated at 200 keV, using a slightly off zone-axis beam. The sample temperature was controlled during irradiation using a Gatan 652 double-tilt heating holder. High-angle annular dark-field (HAADF) TEM images of the as-received material were collected on a JEOL JEM-2100F microscope.

Samples were implanted with 6 keV He^+ ions to a dose of 2×10^{17} ions/cm^2. Ion stopping distributions were calculated (for low helium concentrations) using the software package SRIM [19]. The depth of the helium distribution's maximum was predicted to be 19 and 26 nm for WC and FeCr, i.e. well within the TEM foil thickness. The corresponding maxima in injected helium and displacements per atom (dpa) are reported in Table 1, alongside values for one year of neutron irradiation under a fusion relevant spectrum, as calculated using the FISPACT-II code [20]. The peak ion damage was approximately 15 dpa for both phases, which is comparable to one year of neutron damage (10–16 dpa). The maximum amount of helium introduced, if fully retained – i.e. not redistributed or lost from the foil edges – would correspond to ~50 at. %. Thus, the amounts of He introduced here are far in excess of the predicted annual He production from neutron irradiation alone (~0.02 at. %). Instead, they more closely resemble the direct injection of helium ash in the near surface region from the fusion plasma.

We first report the structure of the un-irradiated material as observed in the TEM. Fig. 1 contains a HAADF image in the top-left, showing heavier elements, i.e. WC particles, in bright contrast and lighter elements, i.e. FeCr binder, in dark. The WC particles are ~0.5–1 µm in diameter. Turning to the EDS maps in the smaller boxes, two other phases are distinguishable, in addition to the nominal constituents. Firstly, in the Cr-map, there are four regions of ~100 nm in diameter, delineated by dotted circles, where the Cr-content is high. Semi-quantitative chemical analysis estimates the Cr-enrichment to be ~10-fold higher than the binder. The significant carbon content, and negligible W or Fe in these particles suggest they are Cr-carbide,
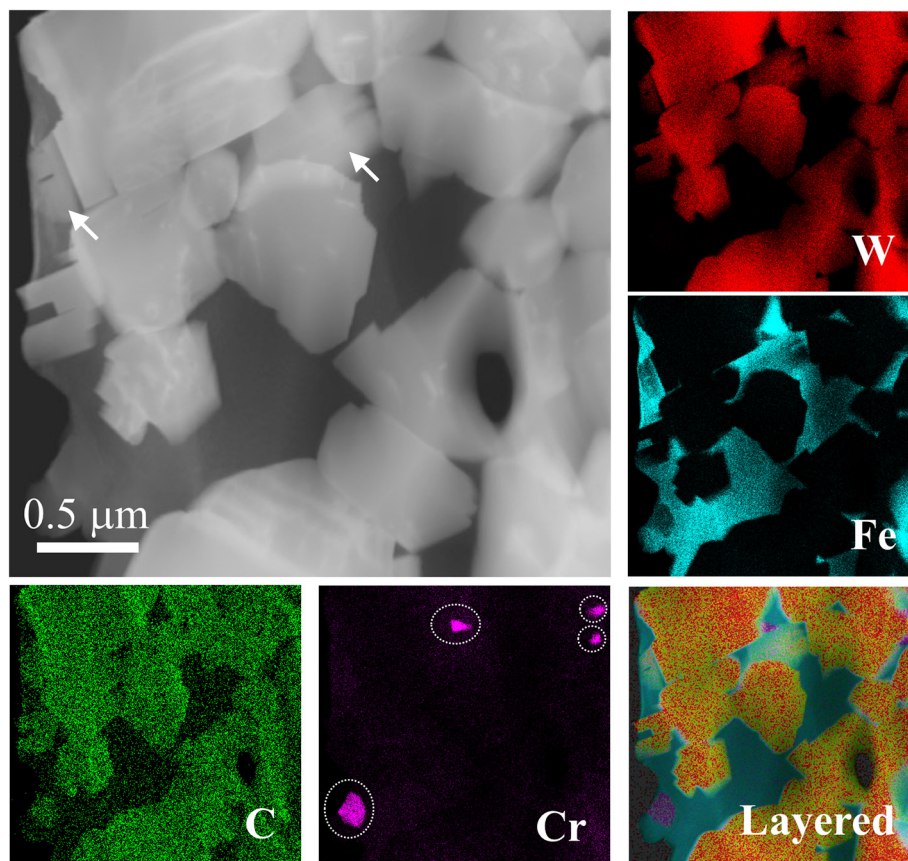

Fig. 1. Top left - HAADF image of the as-received material showing WC (light) and FeCr (dark). Smaller images - EDS dot maps showing W (red), Fe (blue), Cr (purple), C (green) and their sum (Layered). Cr-carbides are indicated by dotted circles and M_6C by arrows.

and we refer to them as such. Secondly, looking at the morphology of light particles in the HAADF image, some (indicated by arrows) have a facetted growth morphology, suggesting they have grown from a liquid during sintering. The maps show that these regions are depleted in W and enriched in Fe with respect to WC. Coupling these observations with prior work on this material in which we observed the $(Fe,W)_6C$ phase via X-ray diffraction at ~2 vol% [21], we shall refer to these particles as M_6C. Having clarified the starting microstructure, we now report the effects of helium damage.

The bubble formations under helium irradiation were markedly different between the WC and FeCr binder. This is evident from Fig. 2, which shows the typical bubble morphology in each phase, as a function of irradiation dose and temperature. We first consider WC. At 25 °C, bubbles only appear at irradiation doses of $>1 \times 10^{17}$ ions/cm^2, and when they do they are fine (~2 nm diameter) – as shown in the magnified region. The size of the bubbles in WC does not appear to coarsen with increasing temperature.

In the FeCr phase, bubbles are observed at markedly lower irradiation doses, appearing at $<5 \times 10^{16}$ ions/cm^2. They are significantly larger and coarsen more at higher temperature. For example, at 25 °C, bubbles of diameter about 3 nm are seen, while at 500 °C, they grow to ~6 nm.

For a more quantitative understanding, Fig. 3 shows bubble size frequency distributions at 2×10^{17} ions/cm^2. In addition to WC and FeCr, the large M_6C precipitates are included (see Fig. 1), however the fine Cr-carbides are excluded, since they were too small to gain reliable measurements. Bubbles were measured by manually tracing >100 bubble perimeters from representative micrographs (shown in the insets) and analysing their area using ImageJ. The resulting spherical-equivalent bubble diameter statistics (mean and standard deviation) are given below the insets.
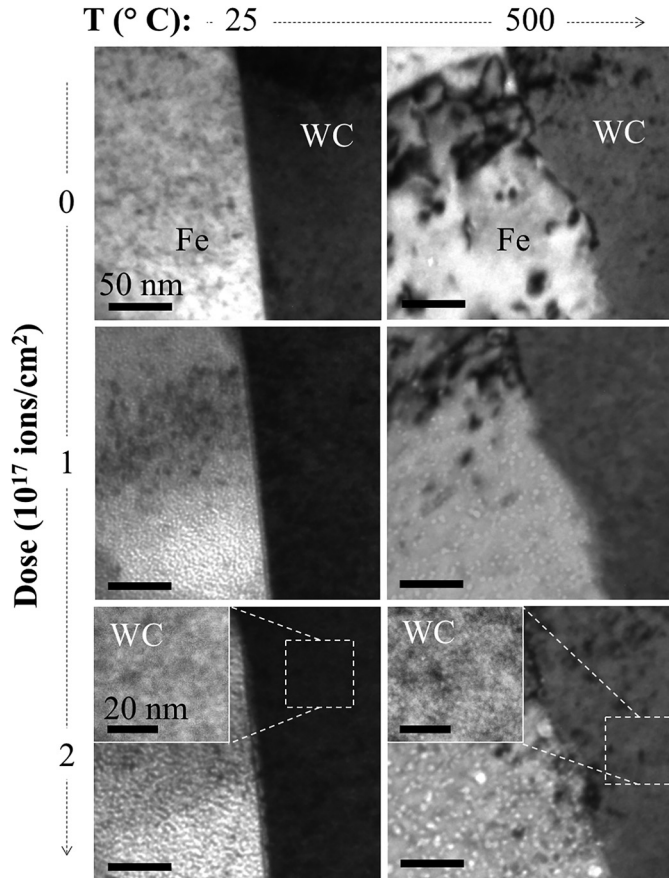

Fig. 3. Frequency distributions of bubble diameter, d, at 2×10^{17} ions/cm^2. WC and M_6C show much finer bubbles with narrower distributions than FeCr. Inset scale bars are 10 nm.

As this is the first report, to our knowledge, of He bubble sizes in WC-based materials, we start our discussion of Fig. 3 on WC and M_6C. The bubble size in these phases is confirmed as very fine (~2 nm) and does not appear to grow significantly at higher irradiation temperature. This suggests that vacancy clusters and/or helium vacancy complexes are relatively immobile at these temperatures, growing in isolation from one another. This is expected on the basis of the expected lattice diffusion rates, D, which can be estimated from the homologous temperature (T/T_m) [22]:

$$D = A \exp(-BT/T_m), \tag{1}$$

where A and B are empirical constants for a given material class (estimated for metal carbides as 0.2 m^2/s and 24 respectively [22]). From D the calculated root-mean-square diffusion distances ($x = \sqrt{Dt}$), where t is the overall irradiation time (~1 h), are given in Table 2. The analysis shows that in WC and M_6C, diffusion distances are always less than the bubble size (e.g. 10^{-11} nm for WC at 500 °C), which supports the idea of isolated bubble growth. The bubble size in WC at 500 °C appears to be

Fig. 2. Typical bubble structures as a function of irradiation temperature and dose. Main image shows WC/FeCr interface with 50 nm scale bars. Magnified areas show bubbles in WC after contrast enhancement (20 nm scale bars).
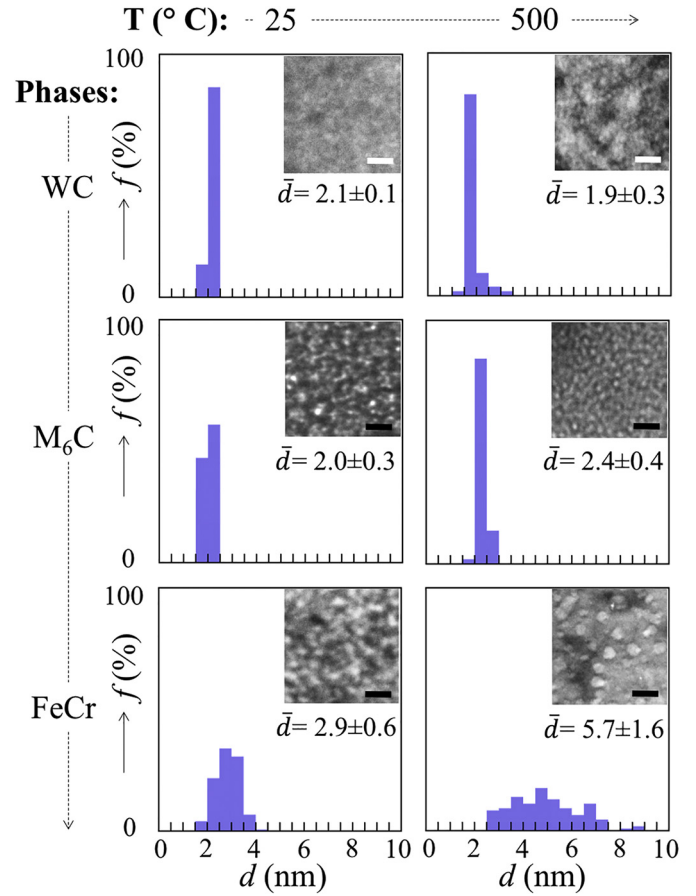
Table 2
Estimated diffusion distances in 1 h for prominent phases at 25 and 500 °C.

Phase	T_m (°C)	T_{25}/T_m	x_{25} (nm)	T_{500}/T_m	x_{500} (nm)
WC	2870	0.09	10^{-45}	0.25	10^{-11}
Fe-8Cr	1170 [16]	0.21	10^{-10}	0.54	10^2
M_6C	1403[a]	0.18	10^{-19}	0.46	10^{-1}

[a] From M_6C liquidus on the WC-10Fe phase diagram at 5.5 wt% carbon [24].

comparable to that in pure W under less extreme conditions. For example, using 15–80 keV He ions, bubbles of 1.1–1.4 nm were seen at 500 °C, at dpas of 0.5–3 and He doses of 0.1–2 at. % [23], i.e. at much lower damage levels and He contents than this study (~15 dpa and 50 at. %). This result shows initial promise for WC-based materials.

In contrast to the carbides, the bubble size in FeCr was significantly larger at 500 °C (5.7 nm) than at 25 °C (2.9 nm). This is indicative of preferential bubble growth, as can be rationalised using the same analysis as above: Employing the constants for BCC transition metals ($A = 1.6$ and $B = 17.8$ [22]), the lattice diffusion distance is estimated to be on the order of 100 nm at 500 °C (see Table 2), which is much greater than the bubble separation, suggesting preferential bubble growth is possible. It is reasonable to compare these observations to ferritic-martensitic steels (typically 8Cr-2W-0.1C) on the basis of their similar crystal structure and contents of dissolved W and C (~4.5 wt% at 700 °C for W and ~0.02 wt% at 900 °C for C [24]). Jia and Dai studied the ferritic-martensic steel F82H, irradiated to 20.3 dpa and 1800 appm He, reporting 1 nm bubbles at 200 °C, which rose sharply to 5 nm at 400 °C [25]. Thus, our observations on the binder & carbide particles are broadly in line with irradiation resistant ferritic-martensitic steels and tungsten, although as we show subsequently, the interfaces between these constituents show unique behaviour.

Interfacial bubble formation is shown in Fig. 4, after a fluence of 2 × 10^17 ions/cm^2 at 25 °C and 500 °C. We first address the observations at 25 °C. Fig. 4(a) is a BF-TEM image showing a large-area view of all phases: three WC particles; a large region of FeCr on the left; a small (<100 nm) Cr-carbide precipitate in the centre; and a region of M₆C in the upper right. The identity of these phases was confirmed with elemental mapping similar to Fig. 1. We can now assess the magnified areas in Fig. 4(b, c). Fig. 4(b) shows a WC/M₆C interface and Fig. 4(c) a WC/Cr-C one. These interfaces are decorated with spherical-cap bubbles that are coarser than those within the respective phases. The bubbles appear adhered to the interface, with the bubbles being capped at the WC side, which is consistent with WC's lower vacancy mobility. What is unexpected about these capped-bubbles is their relative size. In WC/M₆C the bubbles protrude the most and are about 20–40 nm in diameter. In the WC/Cr-C interface, the bubbles protrude to a lesser extent, but were still significant in diameter (10–20 nm). By contrast, in the WC/FeCr interfaces, bubbles were flatter in shape, and only about 5–10 nm in diameter.

Contrary to the behaviour at 25 °C, at 500 °C we found no significant bubble growth at interfaces, despite the growth in bubbles within each phase (see Figs. 2 & 3). Fig. 4(d–f) shows examples of these regions. This could be because of higher mobility for helium within interfaces, leading to rapid helium diffusion and thus possible escape to the specimen surfaces.

The presence of large bubbles on the WC/Cr-carbide and WC/M₆C interfaces at 25 °C is both unexpected, and potentially of engineering consequence. It is unexpected, since the trend is the reverse of what is seen within each phase, where smaller bubbles were seen in M₆C relative to the FeCr binder (see Fig. 3). This is of engineering significance because, if these features pertain under fusion reactor irradiation conditions, they could limit mechanical performance. This implies that, in future development of these materials, the presence of Cr-carbide and M₆C precipitates should be controlled. The Cr-carbides can be reduced by lowering the chromium content of the binder. Coincidentally, the minimum for void swelling in FeCr alloys is thought to occur at 5 wt% [15], suggesting compositions with reduced Cr content are worthy of exploration. The presence of M₆C carbides can similarly be mitigated by making carbon additions during processing. In this study, no graphite additions were made beyond the stoichiometric WC powders, resulting in an overall carbon content of 5.5 wt%, which is well within the conventional two-phase region of the phase diagram for WC-10 wt%Co (i.e. the most common industrial composition), but lies outside the 5.6–5.7 wt% window for the WC-10 wt%Fe system [26]. Carbon corrections should therefore be made accordingly.

The effect of the small spherical-cap bubbles on the WC-FeCr interfaces is unknown. Recent modelling suggests that trapping of He in platelets at incoherent interfaces – which could then later grow to spherical-cap bubbles – could trap He far more efficiently than spherical bubbles alone [27]. It is therefore possible that by controlling the interfacial structure and areal density, irradiation tolerance could be improved, as in the case of dispersion strengthened steels [28], nano-structured metals [29] and metallic multilayers [30]. Nanostructured WC-composites [31] could therefore offer another promising avenue to explore.

In summary, we report He ion irradiations of WC-FeCr to very high (~50 at. %) He contents, corresponding to the regime of direct plasma injection in the near surface region. The FeCr phase grew a coarse array of bubbles, which underwent preferential growth at 500 °C. The WC phase formed a much finer array of uniformly sized bubbles that were stable at both irradiation temperatures. At the interfaces, some surprising features were observed. Spherical-cap bubbles were observed at WC/M₆C and WC/Cr-C interfaces, which were much larger than on WC/FeCr interfaces. This result is unexpected since the bubbles within the respective phases showed the reverse trend. Our observations suggest future studies should investigate in detail the interfacial structure and elimination of tertiary phases.
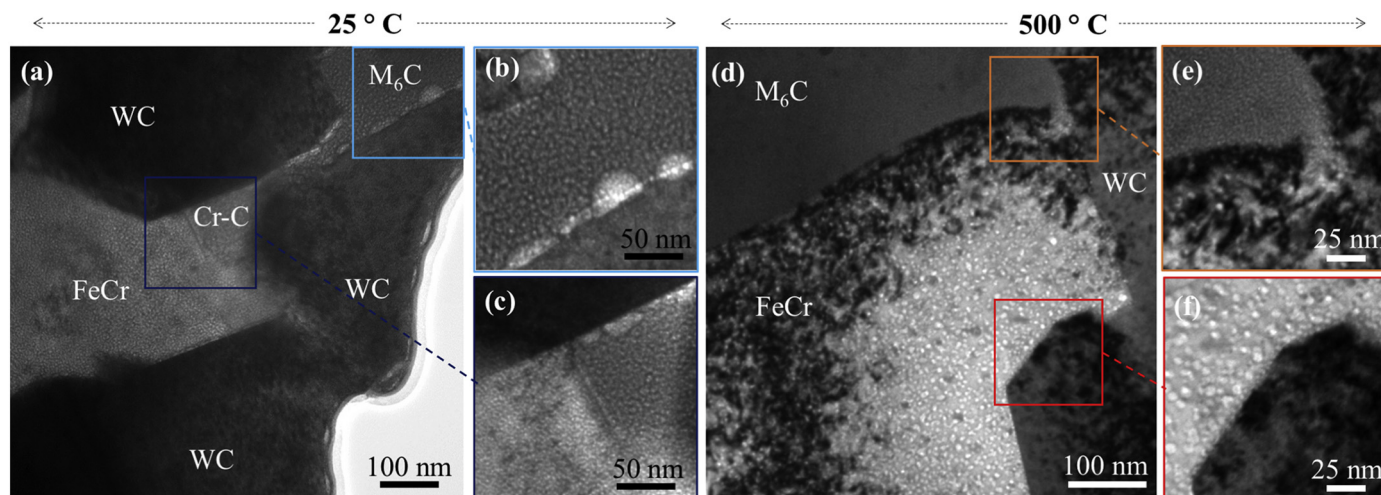

Fig. 4. BFTEM images of interfaces at 25 °C (a–c): (a) large area; (b) underfocus close-up of WC/M₆C; (c) of WC/FeCr/Cr-C region. (d–f) interfaces at 500 °C: (d) large area; (e, f) WC/M₆C and WC/FeCr interfaces respectively.

References

[1] B. Gludovatz, S. Wurster, A. Hoffmann, R. Pippan, ICF12 Ott. 2009, 2012.
[2] J. Riesch, T. Höschen, C. Linsmeier, S. Wurster, J.-H. You, Phys. Scr. 2014 (2014) 014031.
[3] R. Neu, H. Maier, M. Balden, S. Elgeti, H. Gietl, H. Greuner, A. Herrmann, A. Houben, V. Rohde, B. Sieglin, Fusion Eng. Des. 124 (2017) 450–454.
[4] J. Reiser, M. Rieth, B. Dafferner, A. Hoffmann, J. Nucl. Mater. 423 (2012) 1–8.
[5] C.G. Windsor, J.G. Morgan, P.F. Buxton, A.E. Costley, G.D.W. Smith, A. Sykes, Nucl. Fusion 57 (2016), 036001.
[6] B. Roebuck, E.A. Almond, Int. Mater. Rev. 33 (1988) 90–112.
[7] Y. Dai, G.R. Odette, T. Yamamoto, in: R.J.M. Konings (Ed.), Compr. Nucl. Mater, Elsevier, Oxford 2012, pp. 141–193.
[8] C.J. McHargue, Int. Met. Rev. 31 (1986) 49–76.
[9] A. Singh, T.E. Derry, S.B. Luyckx, J.P.F. Sellschop, J. Mater. Sci. Lett. 9 (1990) 1101–1102.
[10] J. Greggi, Scr. Metall. 17 (1983) 765–768.
[11] S.-I. Baik, E.-G. Choi, J.-H. Jun, Y.-W. Kim, Scr. Mater. 58 (2008) 614–617.
[12] J.H. Fremlin, N.A. Askouri, Nature 249 (1974) 137.
[13] N.A. Askouri, J.H. Fremlin, Met. Technol. 2 (1975) 538–541.
[14] A. Prokhodtseva, B. Décamps, A. Ramar, R. Schäublin, Acta Mater. 61 (2013) 6958–6971.
[15] A. Bhattacharya, E. Meslin, J. Henry, A. Barbu, S. Poissonnet, B. Décamps, Acta Mater. 108 (2016) 241–251.
[16] S.A. Humphry-Baker, J.M. Marshall, G.D.W. Smith, W.E. Lee, Proc. 19th Int. Plansee Semin. Reutte Austria, 2017 (HM 19).
[17] A. Kohyama, A. Hishinuma, D.S. Gelles, R.L. Klueh, W. Dietz, K. Ehrlich, J. Nucl. Mater. 233 (1996) 138–147.
[18] J.A. Hinks, J.A. van den Berg, S.E. Donnelly, J. Vac. Sci. Technol. 29 (2011) 021003.
[19] J.F. Ziegler, J. Appl. Phys. 85 (1999) 1249–1272.
[20] J.-C. Sublet, J.W. Eastwood, J.G. Morgan, M.R. Gilbert, M. Fleming, W. Arter, Nucl. Data Sheets 139 (2017) 77–137.
[21] S.A. Humphry-Baker, K. Peng, W.E. Lee, Int. J. Refract. Met. Hard Mater. 66 (2017) 135–143.
[22] A.M. Brown, M.F. Ashby, Acta Metall. 28 (1980) 1085–1101.
[23] R.W. Harrison, G. Greaves, J.A. Hinks, S.E. Donnelly, J. Nucl. Mater. 495 (2017) 492.
[24] C.M. Fernandes, A.M.R. Senos, Int. J. Refract. Met. Hard Mater. 29 (2011) 405–418.
[25] X. Jia, Y. Dai, J. Nucl. Mater. 356 (2006) 105–111.
[26] A. Guillermet, Z. Met. 80 (1989).
[27] A. Kashinath, A. Misra, M.J. Demkowicz, Phys. Rev. Lett. 110 (2013) 086101.
[28] G.R. Odette, Scr. Mater. 143 (2018) 142–148.
[29] S. Wurster, R. Pippan, Scr. Mater. 60 (2009) 1083–1087.
[30] X. Zhang, E.G. Fu, A. Misra, M.J. Demkowicz, JOM 62 (2010) 75–78.
[31] F.L. Zhang, C.Y. Wang, M. Zhu, Scr. Mater. 49 (2003) 1123–1128.